

# Development and Implementation of an Advanced User Material Model for UHMWPE

J.S. Bergström<sup>1</sup>, A.E. Bowden<sup>2,3</sup>, C.M. Rimnac<sup>4</sup>, S.M. Kurtz<sup>2,3</sup>

<sup>1</sup>Exponent, Inc., 21 Strathmore Rd, Natick, MA

<sup>2</sup>Exponent, Inc., 3401 Market Street, Philadelphia, PA

<sup>3</sup>Implant Research Center, School of Biomedical Engineering, Science and Health Systems, Drexel University, 3141 Chestnut St., Philadelphia PA

<sup>4</sup>Musculoskeletal Mechanics and Materials Laboratories,  
Departments of Mechanical and Aerospace Engineering and Orthopaedics,  
Case Western Reserve University, Cleveland, OH

## Abstract

*Ultra-high molecular weight polyethylene (UHMWPE) is a semi-crystalline polymer with excellent strength, impact resistance, and abrasion resistance. These mechanical properties have led to extensive use of UHMWPE as a bearing material in total joint replacements. In order to accurately capture the experimentally observed response of this important polymer we have developed a new advanced material model—the Hybrid Model (HM). This constitutive model is physically motivated and based on a decomposition of the deformation gradient into elastic and viscoplastic components. The elastic response of the underlying molecular network is captured using the eight-chain hyperelastic model, and the viscoplastic response is represented using energy activated flow driven by the molecular reorganization that occurs during large deformations.*

*The constitutive theory for the HM has been implemented as a user-material model (UMAT) for ls971 and is available for both explicit and implicit simulations. For optimal accuracy and numerical efficiency the UMAT uses a forward Euler integration scheme for explicit simulations, and a higher order backward differentiation formula (BDF) method for implicit simulations.*

*The HM was calibrated to data from uniaxial tension experiments performed at different strain rates and with different loading-unloading segments. For validation, the calibrated HM was then used to simulate a small punch test. A direct comparison between the experimental data and model predictions of the calibration and validation data demonstrate that the HM accurately captures the non-linear response of UHMWPE. The ability to simulate large-scale contact problems was examined by simulating the deformation behavior of a total knee replacement component and the Charité™ artificial discs.*

## Introduction

The mechanical behavior of ultra-high molecular weight polyethylene (UHMWPE) is characterized by excellent strength, fatigue, and abrasion resistance. These properties have made UHMWPE an important material for total joint replacements. As an example, every year more than 1 million patients worldwide undergo total joint replacement surgery [1]. It has been shown that the lifetime of the implants can be directly related to the viscoplastic flow of the UHMWPE in the implant components. To better understand and predict component behavior it is important to be able to accurately predict the multiaxial loading response of UHMWPE. For this reason we have in this project developed a new constitutive model framework that incorporates the initial linear elastic response, distributed yielding, large scale yielding, and strain stiffening at large strains – all of which are important characteristics of the experimental response of UHMWPE. The new constitutive model, the hybrid model (HM), is micromechanism inspired and builds upon prior models for glassy, semi-crystalline polymers [2,3,4].

The goal of the present study is to refine our previous work on the HM [5], and to demonstrate the accuracy and usability of the new implementation of the HM as a user-material (UMAT) for LS-DYNA. Techniques for calibrating and validating the HM are presented, together with results from large-scale contact simulations of a total knee replacement component and an artificial disc.

## Constitutive Model Theory

The hybrid model (HM) is an advanced material model specifically developed for predicting the large strain time-dependent behavior of crosslinked and uncrosslinked UHMWPE. The kinematic framework used in the HM is based on a decomposition of the applied deformation gradient into elastic and viscoplastic components:  $\mathbf{F} = \mathbf{F}^e \mathbf{F}^p$  (Figure 1).

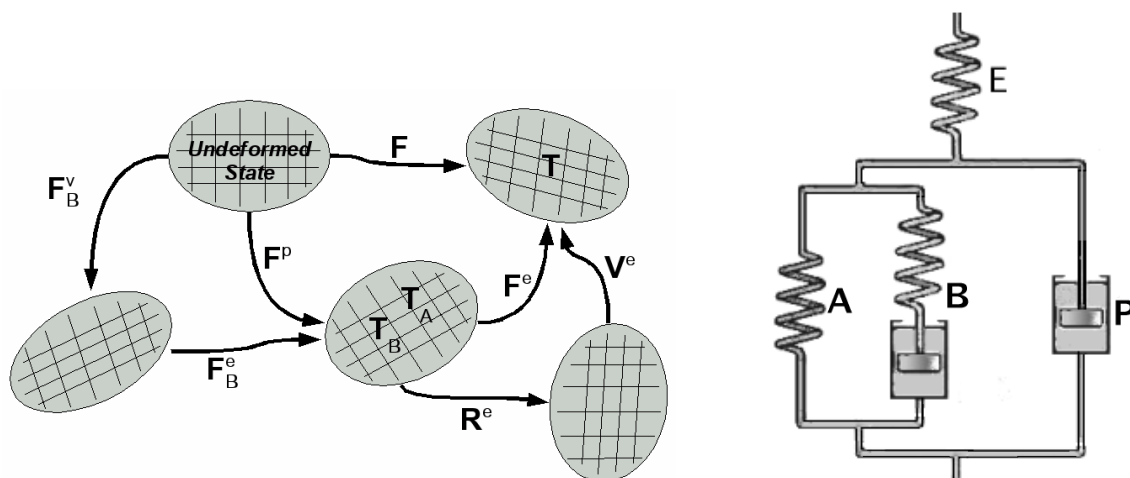


Figure 1. Deformation map and rheological representation of the Hybrid Model.

The spring and dashpot representation shown in Figure 1 is a one-dimensional embodiment of the model framework illustrating that the deformation state is decomposed into elastic ( $E$ ), backstress ( $A, B$ ), and viscoplastic components ( $P$ ).

The Cauchy stress for a given deformation state is given by the isotropic linear elastic relationship:

$$\mathbf{T} = \frac{1}{J^e} (2\mu \mathbf{E}^e + \lambda \operatorname{tr}[\mathbf{E}^e] \mathbf{1}), \quad (1)$$

where  $\mathbf{V}^e$  is the left stretch tensor which can be obtained from the polar decomposition of  $\mathbf{F}^e$ ,  $\mathbf{E}^e = \ln[\mathbf{V}^e]$  is the logarithmic true strain,  $J^e = \det[\mathbf{F}^e]$  is the relative volume change,  $\mu$  and  $\lambda$  are Lame's constants which can be obtained from the Young's modulus ( $E$ ) and Poisson's ratio ( $\nu$ ) by  $\mu = E / (2(1+\nu))$  and  $\lambda = Ev / ((1+\nu)(1-2\nu))$ .

The stress acting on the equilibrium portion of the backstress network ( $A$ ) is given by the 8-chain model [4]:

$$\mathbf{T}_A = \frac{\underline{\mu}_A}{\bar{\lambda}_A} \cdot \frac{L^{-1}(\bar{\lambda}_A / \lambda^{lock})}{L^{-1}(1/\lambda^{lock})} \operatorname{dev}[\mathbf{B}^{P*}] + \kappa [J - 1]^2 \mathbf{1}, \quad (2)$$

where  $\mathbf{B}^{P*} = (J^P)^{-2/3} \mathbf{F}^P (\mathbf{F}^P)^T$  is the distortional portion of the left Cauchy-Green deformation tensor,  $J^P = \det[\mathbf{F}^P]$ ,  $\bar{\lambda}_A = \sqrt{\operatorname{tr}[\mathbf{B}^{P*}]}/3$  is the chain stretch,  $\mu$  is the shear modulus,  $\lambda^{lock}$  is the locking stretch, and  $\kappa = E/(3(1-2\nu))$  is the bulk modulus. The function  $L^{-1}(x)$  is the inverse Langevin function that can be approximated [4] by:

$$L^{-1}(x) = \begin{cases} 1.31446 \cdot \tan(1.58956x) + 0.91209x, & \text{if } |x| < 0.84136 \\ \frac{1}{\operatorname{sign}(x) - x}, & \text{if } 0.84136 \leq |x| < 1 \end{cases} \quad (3)$$

The kinematics of the viscoplastic flow of the backstress network ( $B$ ) is represented by a decomposition of the deformation gradient into elastic and viscoelastic components:  $\mathbf{F}^P = \mathbf{F}_B^e \mathbf{F}_B^v$ , the rate of viscoplastic flow is controlled by energy activated micromechanisms. The stress driving the viscoplastic flow of the backstress network is obtained from the same hyperelastic representation that was used to calculate the backstress, and is similar in structure to the framework used in the Bergström-Boyce representation of crosslinked polymers at high temperatures [4]:

$$\mathbf{T}_B = s_B \cdot \frac{\underline{\mu}}{\bar{\lambda}_B^e} \cdot \frac{L^{-1}(\bar{\lambda}_B^e / \lambda^{lock})}{L^{-1}(1/\lambda^{lock})} \operatorname{dev}[\mathbf{B}_B^{e*}] + \kappa [J - 1]^2 \mathbf{1}, \quad (4)$$

where  $\mathbf{B}_B^{e*} = (J_B^e)^{-2/3} \mathbf{F}_B^e (\mathbf{F}_B^e)^T$ ,  $J_B^e = \det[\mathbf{F}_B^e]$ ,  $\bar{\lambda}_B^e = \sqrt{\operatorname{tr}[\mathbf{B}_B^{e*}]}/3$ , and  $s_B$  is a dimensionless material parameter specifying the relative stiffness of the backstress network.

At small deformations the stiffness of the backstress network is constant and the material response is linear. At intermediate applied deformations, viscoplastic flow caused by molecular chain sliding is initiated. With increasing viscoplastic flow, the crystalline domains become distorted and provide additional molecular material to the backstress network. This is manifested by an initial reduction in the effective stiffness of the backstress network with imposed

viscoplastic deformation and is captured in the model by allowing the parameter  $s_B$  to evolve during the plastic deformation to capture the distributed yielding:

$$\dot{s}_B = -\alpha_B \cdot (s_B - s_{Bf}) \cdot \dot{\gamma}_P, \quad (5)$$

where  $\alpha_B$  is a material parameter specifying the transition rate of the distributed yielding event,  $s_{Bf}$  is the final value that  $s_B$  reaches at fully developed plastic flow, and  $\dot{\gamma}_P$  is the magnitude of the viscoplastic flow rate (Equation (7)).

The velocity gradient of the viscoelastic flow of the backstress network is given by [5]:

$$\mathbf{L}_B^v = \dot{\gamma}_0 \left( \frac{\tau_B}{\tau_B^{base} \cdot [1 + p_B / \hat{p}]} \right)^{m_B} \mathbf{F}_B^{e-1} \frac{\text{dev}[\mathbf{T}_B]}{\tau_B} \mathbf{F}_B^e. \quad (6)$$

In this equation  $p_B = -\text{tr}[\mathbf{T}_B]/3$  is the hydrostatic pressure,  $\hat{p}$  is a material parameter specifying the pressure dependence of the yield stress,  $\tau_B = \|\text{dev}[\mathbf{T}_B]\|_F$  is the Frobenius norm of the deviatoric part of  $\mathbf{T}_B$ ,  $\tau_B^{base}$  and  $m_B$  are material parameters, and  $\dot{\gamma}_0 \equiv 1/s$  is a constant that is introduced for dimensional consistency.

The yielding and plastic flow of the material is captured using a similar energy activation approach as was used for the flow of the backstress network:

$$\mathbf{L}^p = \dot{\gamma}_p \mathbf{R}^{eT} \frac{\text{dev}[\mathbf{T}_p]}{\tau_p} \mathbf{R}^e = \dot{\gamma}_0 \cdot \left( \frac{\tau_p}{\tau_p^{base} \cdot [1 + p_p / \hat{p}]} \right)^{m_p} \mathbf{R}^{eT} \frac{\text{dev}[\mathbf{T}_p]}{\tau_p} \mathbf{R}^e, \quad (7)$$

where  $\mathbf{L}^p = \dot{\mathbf{F}}^p \mathbf{F}^{p-1}$  is the velocity gradient,  $\mathbf{T}_p = \mathbf{T} - \mathbf{F}^e (\mathbf{T}_A + \mathbf{T}_B) \mathbf{F}^{eT} / J^e$  is the stress acting on the relaxed configuration convected to the current configuration,  $\tau_p = \|\text{dev}[\mathbf{T}_p]\|_F$  is the effective shear stress (calculated using the Frobenius norm) driving the viscoplastic flow,  $p_p = -\text{tr}[\mathbf{T}_p]/3$  is the hydrostatic pressure,  $\tau_p^{base}$ ,  $\hat{p}$ , and  $m_p$  are material parameters, and  $\dot{\gamma}_0 \equiv 1/s$  a constant that is introduced for dimensional consistence.

In total, the HM contains 13 material parameters: 2 small strain elastic constants ( $E_e, v_e$ ); 2 hyperelastic constants for the back stress network ( $\mu_A, \lambda_A^{lock}$ ); 6 flow constants of the backstress network ( $s_{Bi}, s_{Bf}, \alpha_B, \tau_B^{base}, m_B, \hat{p}$ ); and 2 yield and viscoplastic flow parameters ( $\tau_p^{base}, m_p$ ).

## Numerical Integration Algorithm

The structure of the constitutive equations for the hybrid model (HM) constitutes a system of coupled ordinary differential equations. Solving these constitutive equations in a finite element setting requires a careful integration scheme. The following algorithm illustrates a simple and effective approach for updating the stress and state variables in an increment from time  $t$  to time  $t + \Delta t$ .

Table 1. Algorithm used to integrate the hybrid model.

1	Known state variables at time $t$ : $\mathbf{F}(t), \mathbf{F}^P(t), \mathbf{F}_B^v(t), s_B(t)$
2	Known applied deformation at time $t + \Delta t$ : $\mathbf{F}(t + \Delta t)$
3	For any time $\hat{t}$ between $t$ and $t + \Delta t$ , let: $\mathbf{F}(\hat{t}) = \mathbf{F}(t) + \frac{\hat{t} - t}{\Delta t} \cdot [\mathbf{F}(t + \Delta t) - \mathbf{F}(t)] \quad (8)$
4	Collect all state variables in to an array $\xi$ : $\xi \equiv [\mathbf{F}^P; \mathbf{F}^v; s_B] = [F_{ij}^P; F_{kl}^v; s_B], \text{ where } i,j = 1, 2, 3 \text{ and } k,l = 1, 2, 3$
5	The rates of change of the state variables are given by: $\dot{\mathbf{F}}^P = \mathbf{L}^P \mathbf{F}^{P-1} = \dot{\gamma}_0 \cdot \left( \frac{\tau_p}{\tau_p^{base} \cdot [1 + p_p / \hat{p}]} \right)^{m_p} \left[ \mathbf{R}^{eT} \frac{\text{dev}[\mathbf{T}_p]}{\tau_c} \mathbf{R}^e \right] \mathbf{F}^{P-1} \quad (9)$ $\dot{\mathbf{F}}_B^v = \mathbf{L}_B^v \mathbf{F}_B^{v-1} = \dot{\gamma}_0 \cdot \left( \frac{\tau_B}{\tau_B^{base} \cdot [1 + p_B / \hat{p}]} \right)^{m_B} \left[ \mathbf{F}_B^{e-1} \frac{\text{dev}[\mathbf{T}_B]}{\tau_B} \mathbf{F}_B^e \right] \mathbf{F}_B^{v-1} \quad (10)$ $\dot{s}_B = -\alpha_B \cdot (s_B - s_{Bf}) \cdot \dot{\gamma}_0 \cdot \left[ \frac{\tau_p}{\tau_p^{base} (1 + p_p / \hat{p})} \right]^{m_p} \quad (11)$ These equations can be written in vector form: $\dot{\xi}_i = f(\xi_1, \xi_2, \dots, \xi_N, t), \quad (12)$ where $N=19$ is the number of state variables.
6	The set of differential equation in Equation (12) can be solved using standard solution methods. For explicit simulations, where the time increment size is always very small, the equations can effectively be solved using a forward Euler approach: $\dot{\xi}_i(t + \Delta t) = \dot{\xi}_i(t) + \Delta t \cdot \dot{\xi}_i(t).$ For implicit simulations it is desirable to have a large time step size. For this reason it is advantageous to use a higher-order differential equation solver. In this project we have used a variable-order, variable step-size, Adams predictor-corrector method [6,7,8] to solve the equations in implicit simulations.

## Materials and Methods

The user-material (UMAT) implementation of the hybrid model (HM) was calibrated using uniaxial monotonic tension and uniaxial cyclic loading results. The experimental data was obtained using ram-extruded rods of UHMWPE (GUR1050) [5]. The material was gamma irradiated with a dose of 100 kGy, and then heat treated at 110°C for two hours. The degree of crystallinity of the material, as determined by differential scanning calorimetry, was 0.61 [5].

Specimens from the crosslinked material were tested at room temperature in uniaxial tension (Figure 2). The specimens had a diameter of 10 mm and a gauge length of 25 mm. The strain was measured using a non-contacting video extensometer. The true-stress and true-strain were computed from the force-extension data assuming a homogeneous isochoric deformation field.

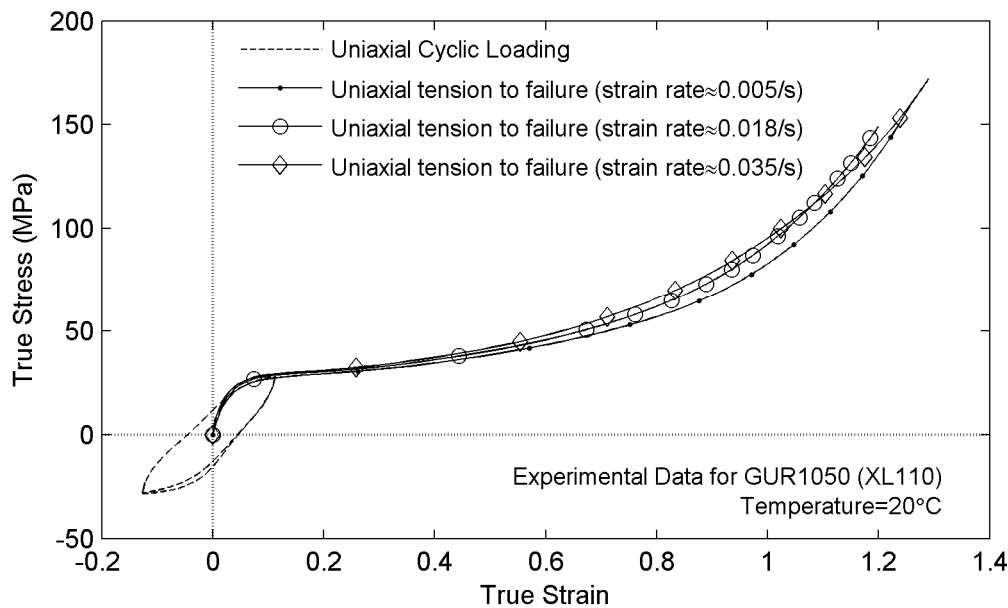


Figure 2. Uniaxial tensile data used for calibrating the hybrid model.

For validation purposes, the UHMWPE material was also loaded using a small punch test setup. In these tests, disc-shaped specimens with a diameter of 6.4 mm and a thickness of 0.5 mm were tested by indentation with a hemispherical punch head at a constant displacement rate of 0.5 mm/min. The results from the punch test, together with a schematic of the setup are shown in Figure 3.

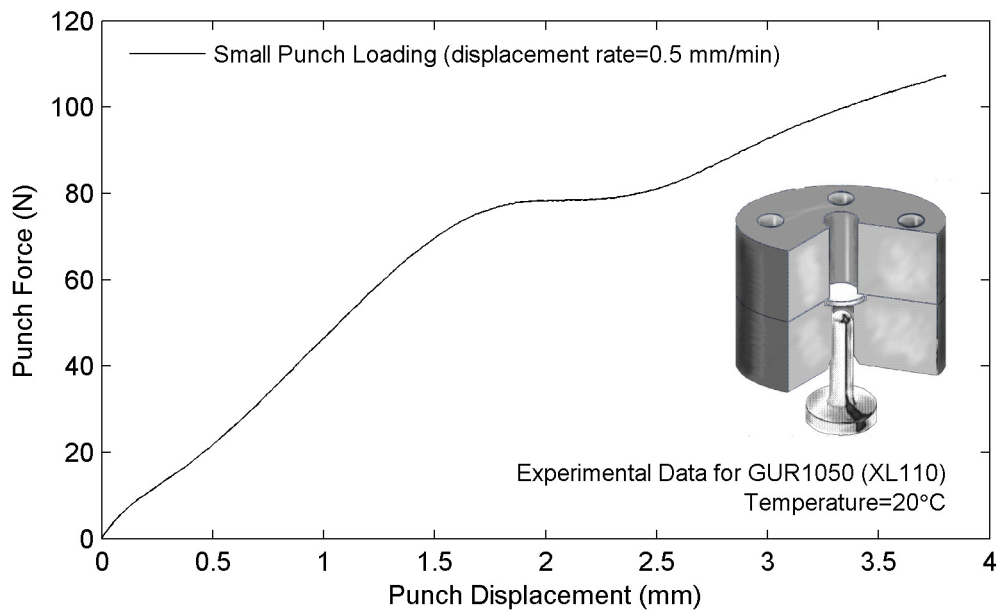


Figure 3. Small punch experimental data used for validation of the hybrid model.

## Results

The hybrid model (HM) was calibrated to the uniaxial experimental data shown in Figure 1. The optimal material parameters giving the highest coefficient of determination  $R^2$  were found using a custom computer program written in Matlab®. The computer program used an iterative procedure based on the Nelder-Mead simplex algorithm. The optimal set of material parameters is summarized in Table 2, and the predicted stress-strain curves from the calibration are shown in Figures 4 and 5. These figures demonstrate that the HM is capable of predicting both large strain uniaxial loading at different strain rates, and small strain cyclic loading.

Table 2. Optimal material parameters for the UHMWPE material.

Material Parameter	GUR 1050 (100 kGy $\gamma$ 110°C)
$E$ (MPa)	2452
$\nu$	0.46
$\mu_A$ (MPa)	9.21
$\lambda_A^{lock}$	2.83
$s_{Bi}$	40.0
$s_{Bf}$	10.0
$\alpha_B$	27.0
$\tau_B^{base}$ (MPa)	24.6
$m_B$	9.50
$\hat{p}$ (MPa)	200
$\tau_p^{base}$ (MPa)	8.00
$m_P$	3.30

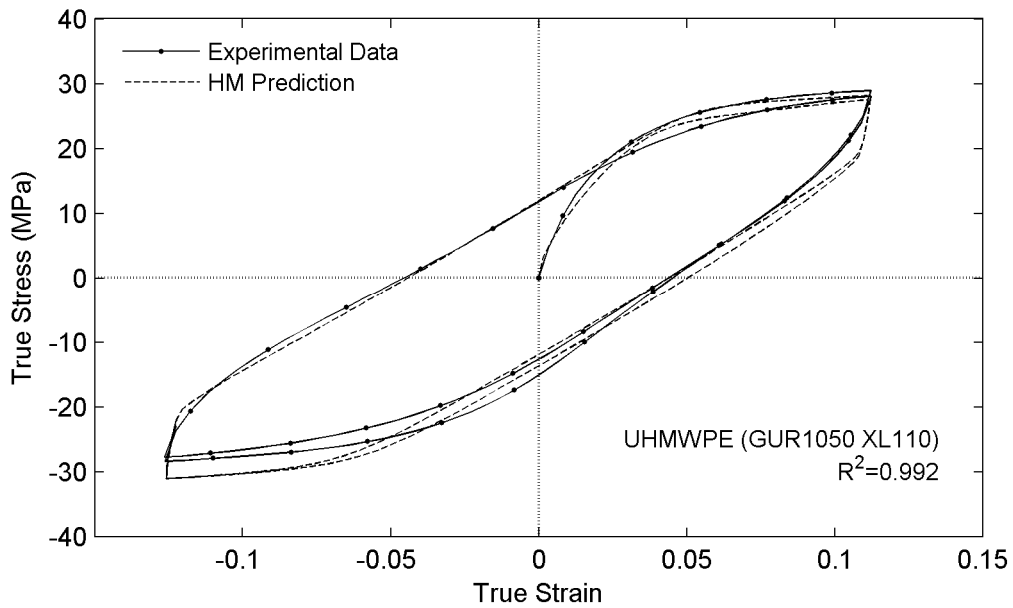


Figure 4. Comparison between uniaxial cyclic experimental data for UHMWPE and LS-DYNA predictions using the hybrid model.

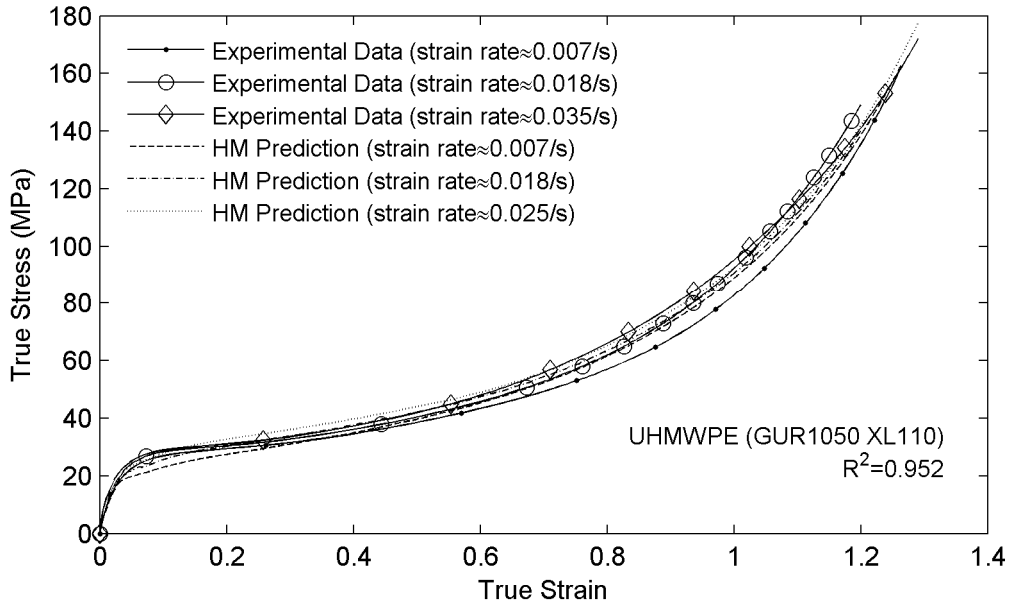


Figure 5. Comparison between monotonic uniaxial experimental data for UHMWPE and LS-DYNA predictions using the hybrid model.

The calibrated HM was then used to predict the response from the small punch test. The results from the small punch simulation, together with the FE mesh, are presented in Figure 6. This figure shows that the calibrated HM can also accurately predict the response of the multiaxial deformations history applied in the small punch test.

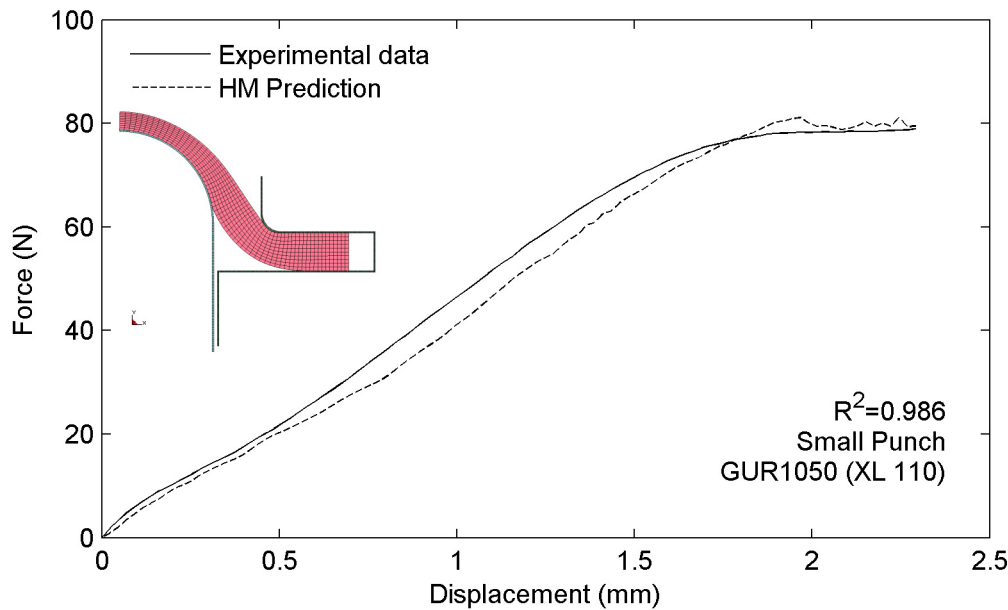


Figure 6. Comparison between small punch experimental data for UHMWPE and LS-DYNA predictions using the hybrid model.

To illustrate the usefulness of the user material model to solve large-scale simulations with contact, two 3D test cases performed. The first case (Figure 7) shows the deformation of a total knee replacement component under contact loading with a stabilizing post. This simulation was performed using an implicit solution approach.

A second example is shown in Figure 8. This figure shows the sliding deformation and accompanying Mises stress field in a Charité™ artificial disc. This simulation was performed using an explicit solution approach.

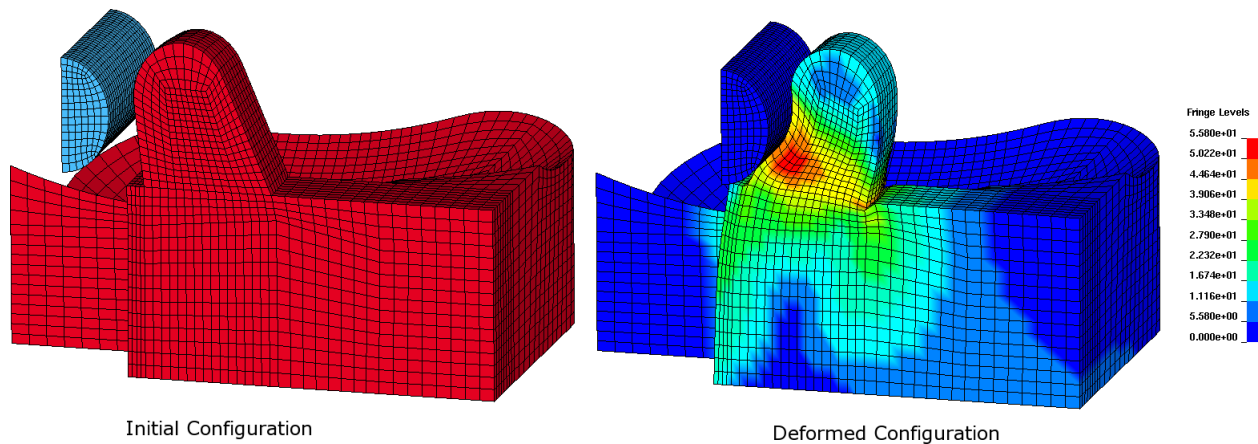


Figure 7. Finite element results from a 3D simulation of a total knee replacement component. The mesh contains 27,000 elements.

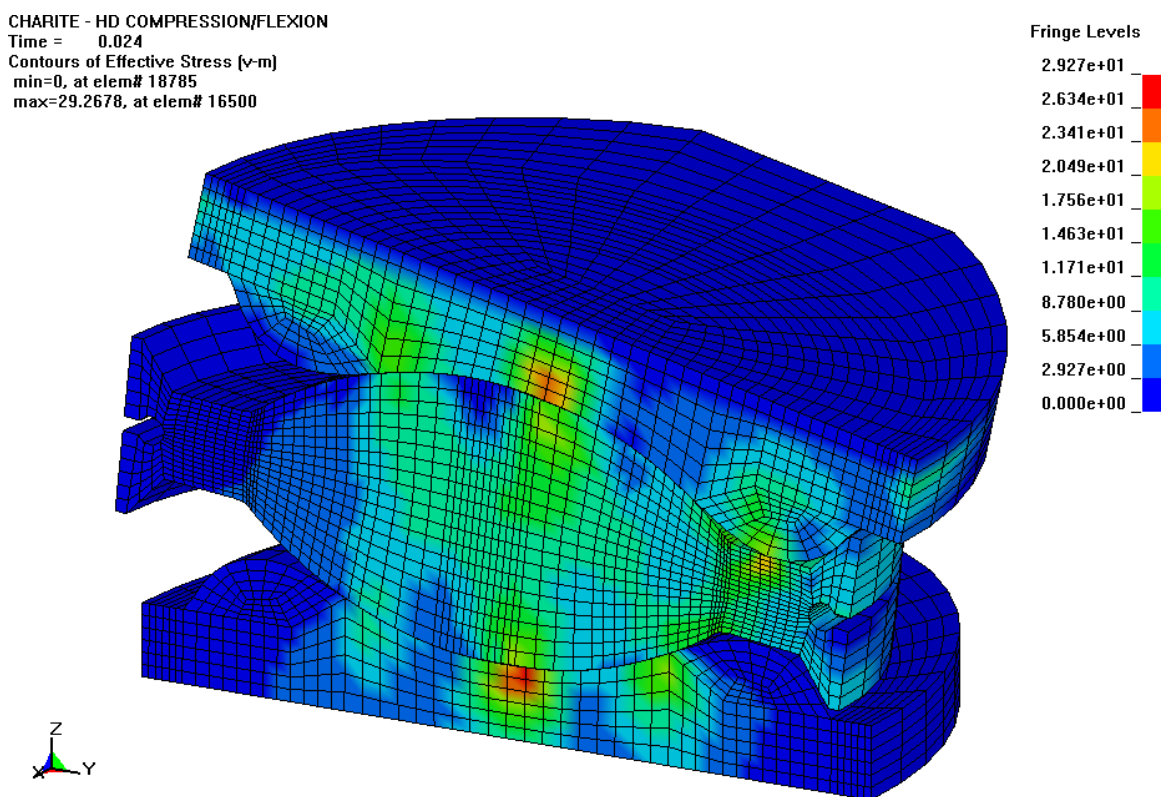


Figure 8. Finite element results showing contours of Mises stress from a 3D simulation of the Charité™ artificial discs. The mesh contains 24,000 elements.

## Discussion

The uniaxial and multiaxial deformation behavior of UHMWPE has been experimentally studied using monotonic and cyclic loading histories. The experimental characterization together with insights into the micromechanisms controlling the deformation behavior has been used to develop a new advanced constitutive model for UHMWPE. This new model builds upon prior models and is called the hybrid model (HM). As part of this work we have implemented the HM as a user-material model (UMAT) in ls971.

As is shown in Figures 4 to 6, the HM can accurately predict the uniaxial and multiaxial deformation response of UHMWPE. The  $R^2$ -values of the predictions range from 0.95 to 0.99. Figures 7 and 8 also demonstrated that the HM can be used in large-scale LS-DYNA simulations that include contact. The developed material model is a valuable tool that enables accurate predictions of a multitude of advanced real-world problems.

## Acknowledgement

This work was supported by NIH Grant 1 R01 AR 47192.

## References

- [1] Orthopaedic Products. In: Smith RC, Geier MA, Reno J, Sarasohn-Kahn J, editors. Medical & Healthcare Marketplace Guide. New York: IDP Enterprises, L.P. 1998.
- [2] E.M. Arruda, M.C. Boyce, “Effects of strain rate, temperature and thermomechanical coupling on the finite strain deformation of glassy polymers”, Mech Mater, vol. 19, pp. 193-212, 1995.
- [3] O.A. Hasan, M.C. Boyce, “A constitutive model for the nonlinear viscoplastic behavior of glassy polymers”, Polymer Eng. Sci., Vol. 35, pp. 331-344, 1995.
- [4] J.S. Bergstrom, M.C. Boyce, “Constitutive modeling of the time-dependent and cyclic loading of elastomers and application to soft biological tissues”, Vol. 33, pp. 523-530, 2001.
- [5] J.S. Bergstrom, C.M. Rinnac, S.M. Kurtz, “An augmented hybrid constitutive model for simulation of unloading and cyclic loading behavior of conventional and highly crosslinked UHMWPE”, Biomaterials, Vol. 25, pp. 2171-2178, 2004.
- [6] C.W. Gear , “Numerical Initial Value Problems in Ordinary Differential Equations”, Prentice Hall, 1971.
- [7] C.W. Gear, “The automatic integration of ordinary differential equations”, vol. 14 , pp. 176 – 179, 1971.
- [8] A. C. Hindmarsh, “ODEPACK, A Systematized Collection of ODE Solvers,”, in Scientific Computing, R. S. Stepleman et al. (eds.), North-Holland, Amsterdam, 1983 (vol. 1 of IMACS Transactions on Scientific Computation), pp. 55-64.